Heliyon 9 (2023) e18816

Contents lists available at ScienceDirect

Heliyon

journal homepage: www.cell.com/heliyon

Highly efficient and stable lead-free cesium copper halide perovskites for optoelectronic applications: A DFT based study

Md Lokman Ali [a,*], Mithun Khan [a], Md Abdullah Al Asad [b], Md Zahidur Rahaman [c]

[a] Department of Physics, Pabna University of Science and Technology, Pabna, 6600, Bangladesh
[b] Department of Electrical and Electronic Engineering, Bangabandhu Sheikh Mujibur Rahman Science and Technology, Gopalganj, Bangladesh
[c] School of Materials Science and Engineering, Faculty of Science, University of New South Wales, Sydney, 2052, Australia

ARTICLE INFO

Keywords:
First-principles calculations
Structural properties
Optical properties
Electronic properties
Mechanical properties
Thermodynamic properties

ABSTRACT

Recently synthesized industrially significant perovskites $Cs_3Cu_2X_5$ ($X = Cl, Br, I$) are subjected to a density functional theory (DFT) investigation utilizing the CASTEP code. This study explores various physical features, including structural, optical, thermodynamic, elastic, mechanical, and electronic properties. There is a strong correlation between the optimized structure parameters and the existing experimental data, which demonstrates the reliability of our DFT-based computations. The band structure and density of states (TDOS and PDOS) analysis revealed that all the studied perovskites are direct band gap semiconductors, and $Cs_3Cu_2Br_5$ has the smallest band gap (2.092 eV). We also discussed the mechanical and cell stability using the Born stability criterion and formation energy, respectively. The mechanical and dynamic stability of each phase is confirmed by the analysis of the elastic constants. According to the computed values of Pugh's and Poisson's ratios as well as Cauchy's pressure, all of the studied compounds are ductile in nature. The study of density of states, total charge density, and Mulliken atomic populations reveal that all the compounds have complex bonding with both ionic and covalent properties. Finally, utilizing the elastic constant data, the Debye temperatures of $Cs_3Cu_2Cl_5$, $Cs_3Cu_2Br_5$, and $Cs_3Cu_2I_5$ have been determined as 82.90 K, 100.00 K, and 80.70 K, respectively. The analysis of thermodynamics (relatively low values of both Θ_D and K_{min}) as well as optical properties indicate that all the investigated materials have the potential to serve as thermal barrier coating (TBC) materials.

1. Introduction

Halide perovskites have garnered a lot of attention from researchers and specialists throughout the world who work to advance optoelectronic and photovoltaic technology. The materials are intended to be used in various solar and photovoltaic applications due to their predominant physiochemical properties, with an enhanced power conversion efficiency of over 22% [1]. The highest observed PCE is 25.2% for $MAPbI_3$ solar cells [2]. Compared to other materials, perovskites have a higher potential for industrial applications due to their abundance and desirable physical properties, such as a tunable bandgap, strong absorption across a broad spectrum, decreased reflectivity, excellent photoconductivity, high mobility with low carrier effective masses, and long duration charge diffusion paths [3–9]. Perovskite-based solar technology is predicted to be more efficient and less expensive than traditional techniques

* Corresponding author. Pabna University of Science and Technology, Pabna, Bangladesh.
E-mail address: lokman.cu12@gmail.com (M.L. Ali).

https://doi.org/10.1016/j.heliyon.2023.e18816
Received 27 March 2023; Received in revised form 18 July 2023; Accepted 28 July 2023
Available online 29 July 2023

associated with silicon [10]. The halide hybrid perovskites still face many challenges in the commercialization process due to their structural instability and ease of decomposition when exposed to humidity, moisture, temperature, and UV light, despite the tremendous research and technological advancements in this field. Additionally, most of those materials present toxic lead, which seriously impacts our ecosystem [11,12]. Because of this, it is preferred to substitute non-toxic stable alternative elements for to create environmentally perovskites that have comparable optoelectronic properties to lead-based perovskites.

To provide improved stability and reduced toxicity of all inorganic copper-based compounds, researchers started using Cu^{2+} rather than harmful Pb^{2+} [13]. Sn-based perovskite exhibits poor stability among lead-free perovskites and is challenging to use in applications because Sn (II) oxidation is inevitable [14]. Many lead-free halide perovskite materials have been reported since Snaith's team initially used $CH_3NH_3SnI_3$ as photoactive material [15]. These materials are frequently used in solar cells, photodetectors, LEDs, and field-effect transistors (FETs) [15]. Ge-based inorganic perovskites, which have more excellent conductivity and absorption than Pb-based perovskites, are now a potential replacement for Pb. Additionally, they assert that $CsGeI_3$ is the best Pb-free halide material, although it is brittle and $CsGeBr_3$ is ductile [16,17]. Numerous attempts have been done to develop Pb-free perovskites, among the inorganic compounds $Cs_3Bi_2I_9$ [18], $Cs_3Cu_2I_5$ [19,20], $Cs_3Cu_2X_5$ [21–23,24,25], and others, as well as the organic-inorganic (hybrid) compounds $(C_4N_2H_{14}Br)_4SnBr_6$ [26], $(C_9NH_2O)_2SbCl_5$ [27], $[Mn(DMSO)_6]_{14}$ [28], $(C_{18}H_{35}NH_3)_2SnBr_4$ [29] perovskites. In particular, the Cu-based non-toxic zero-dimensional perovskite-like derivatives $Cs_3Cu_2X_5$ $(X = Cl, Br, I)$ with self-trapped exciton photo-luminescence exhibit some excellent characteristics, such as broad emission spectrum, large exciton binding energy, strong photoluminescence, high photoluminescence quantum yield (PLQY), and tunable emission wavelength, which have made outstanding contributions to the field of optoelectronics [21–23,30–32]. Although the synthesis and exceptional properties of low-dimensional copper halides $Cs_3Cu_2X_5$ $(X = Cl, Br, I)$ have been reported recently, a comprehensive theoretical investigation of their physiochemical properties is still lacking.

This paper presents and analyzes various physical properties of a novel class of Cu-based eco-friendly perovskites $Cs_3Cu_2X_5$ $(X = Cl, Br, I)$. Using first-principles DFT computation for the first time, we have researched Pb-free Cu-based halide perovskites $Cs_3Cu_2X_5$ $(X = Cl, Br, I)$ to reveal the features of the materials to attain optimal characteristics suited for optoelectronic and photovoltaic purposes. The structural, optical, electronic, elastic, mechanical, and thermodynamic properties of three Pb-free perovskites were studied. This study will increase understanding of Pb-free Cu-based perovskites and contribute to developing non-toxic Cu-based perovskites for solar cells as well as other optical and electronic applications.

2. Computational methods

A first-principles calculation based on DFT was utilized to investigate the precise physical characteristics of $Cs_3Cu_2X_5$ $(X = Cl, Br, I)$ semiconductors. Using the CASTEP program, the analyses were performed [33–36]. Generalized gradient approximation (GGA) is used to investigate the exchange-correlation energy function created by Perdew, Burke, and Ernzerhof [37]. Pseudoatomic computations were implemented owing to the valence electrons $Cs - 6s^1$, $Cu - 3d^9 4s^2$, $Cl - 3s^2 3p^5$, $Br - 4s^2 4p^5$, and $I - 5s^2 5p^5$ for perovskites $Cs_3Cu_2X_5$ $(X = Cl, Br, I)$ semiconductors. In the optimization case, the Venderbilt-type ultrasoft pseudo-potential was applied to simulate the interactions between ions and electrons in Cs, Cu, Cl, Br, and I [38]. Using the Monkhorst-Pack approach, the k-points sampling located in the Brillouin zone was created in all cases [39]. In all cases, Brillouin zone sampling with k-points $6 \times 6 \times 6$ was used. To expand plane wave functions, 450 eV was used as the cut-off energy. The best atomic positions and lattice properties for every compound were determined using the Broyden-Fletcher-Goldfarb-Shanno (BFGS) scheme [40]. The unit cell and atomic relaxation were measured using 1×10^{-5} eV/atom total energy, 0.03 eV/Å maximum force, 0.001 Å maximum displacement, and 0.05 GPa maximum stress. In order to determine the elastic constants of $Cs_3Cu_2X_5$ $(X = Cl, Br, I)$ semiconductors, the "stress-strain" theory [41] was applied. Voigt-Reuss-Hill (VRH) approximations were used to get the elastic moduli from the elastic constants [42–44].

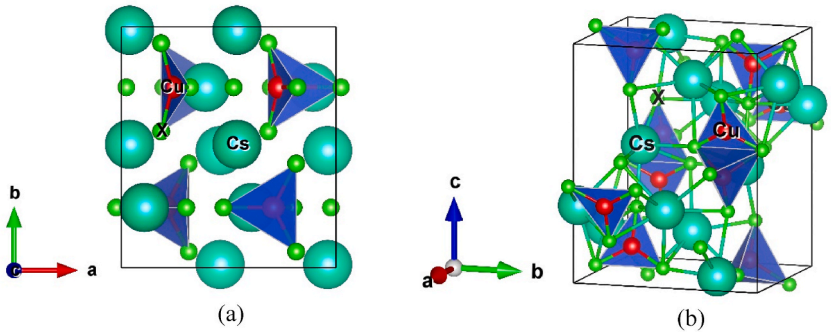

Fig. 1. The lattice consists of (a) two-dimensional chains of $[Cu_2X_5]^{-3}$ units parallel to the c axis, divide by rows of Cs^+ ions and (b) three-dimensional crystal structure of $Cs_3Cu_2X_5$ $(X = Cl, Br, I)$ semiconductors.

3. Results and discussion

3.1. Structural properties

The lead-free Cu-based halide perovskites, $Cs_3Cu_2X_5$ $(X = Cl, Br, and\ I)$, crystallise in the orthorhombic structure with space group *Pnma* (#62) [30–32,45]. There are 40 atoms in a crystallographic unit cell, where 12 Cs atoms in the body-centered position at 1 b Wyckoff point, 8 Cu atoms in the corner-centered position at 1a Wyckoff point, and 20 × atoms holding the side-centered position at 3 d Wyckoff point, with fractional coordinates of (0.0387, 0.9868, 0.679), (0.2077, 0.25, 0.549), and (0.0235, 0.75, 0.4892), respectively [45]. Fig. 1 (a, b) shows the unit cell of a hypothetical perovskite crystal $Cs_3Cu_2X_5$ composed of the elements Cs, Cu, and X (X = Cl, Br, I). Table 1 displays our optimized structural finding and optimal cell volume of $Cs_3Cu_2X_5$ perovskites. In Table 1, we see that the predicted optimized structural parameters for the compounds under study agree very well with the findings of the available experimental research. The structural properties of the investigated compounds are predicted to change regularly due to the periodic replacement of atoms. Our results also imply that the structural characteristics of considered perovskites shift periodically when similar atoms replaced periodically. The replacement of chlorine with bromine and iodine is seen to cause periodic increases in the optimized lattice parameters and unit cell contents [21,30–32,45]. Similarly, the lattice constants are decreased when chlorine and bromine replaced iodine. Consequently, it is desirable to tune the optoelectronic properties due to the periodic change in structural features. We also compute the formation energy for the considered compounds using the following equation (1) to confirm their phase stability [24,25,46].

$$\Delta E_f(Cs_3Cu_2X_5) = \frac{E_{tot}(Cs_3Cu_2X_5) - 12 \times E_s(Cs) - 8 \times E_s(Cu) - 2 \times E_s(X)}{N}; (X = Cl, Br, I) \quad (1)$$

Here, $E_s(Cs)$, $E_s(Cu)$, and $E_s(X)$ denote the energy of the corresponding atoms of *Cs*, *Cu*, and *X*, whereas $E_{tot}(Cs_3Cu_2X_5)$ represents the total energy of $Cs_3Cu_2X_5$, and *N* denotes all the atoms in the unit cell. All of the investigated compounds have negative formation energy values, indicating they are thermodynamically stable.

3.2. Optical properties

The optical properties of the Pb-free inorganic halide perovskites $Cs_3Cu_2X_5$ $(X = Cl, Br, and\ I)$ are studied in the CASTEP module using first-principles DFT calculations for the photon energies ranging 0–30 eV. Optical properties explain how materials behave when exposed to electromagnetic radiation and also describe the material's potential and performance in a device [21–23]. These properties include absorption, dielectric function, conductivity, reflectivity, loss function, and refractive index.

The dielectric function accurately describes the optoelectronic device's response to incident electromagnetic radiation. The real and imaginary dielectric functions were shown in Fig. 2(a) and (b), respectively. Our findings indicate that $Cs_3Cu_2X_5$ have the greatest dielectric constants in the lower-energy area (0–4 eV). However, substituting a halogen atom with another halogen results in a remarkable change in the dielectric function. In the infrared to ultraviolet region of the electromagnetic spectrum, the inorganic compound $Cs_3Cu_2Cl_5$ has the strongest dielectric function, making it better suited for photovoltaic applications [19]. When I is substituted by Br and Cl, the dielectric function value decreases and the peaks shift to the high-energy region of the spectrum.

Optical absorption describes the depth to which incident radiation of a given intensity enters a substance before being absorbed. Fig. 3(a) displays the computed absorbance spectra for the considered $Cs_3Cu_2X_5$ semiconductors. The most significant energy range of absorption is between 2.5 eV and 25 eV. Absorption spectra of $Cs_3Cu_2I_5$ show a maximum initial peak at 8 eV. The results demonstrate that when one halogen is replaced by another, the absorption coefficient changes dramatically, just like the dielectric function. Overall, the substitution of I with Br and Cl pushes the absorption peaks to higher energies with a corresponding decrease in the strength of the first peaks [21].

An essential parameter in photovoltaics is optical conductivity, which provides estimates of photoconductivity. The computed real

Table 1
Ground state structural parameters for $Cs_3Cu_2X_5$ $(X = Cl, Br, and\ I)$.

Materials	*a* (Å)	b (Å)	*c* (Å)	*V* (Å)	ΔE_f (eV)	E_g *(eV)*	Remarks
$Cs_3Cu_2Cl_5$	9.601	10.793	13.598	1409.07	−3.396	2.344	[This work]
	9.279	10.542	13.212	1292.39	−1.565	–	Expt [45].
	9.176	10.505	13.141	1266.71	–	2.450	Expt [30].
	9.572	10.820	13.400	1387.83	–	2.35	Theo [32].
	9.29	10.54	13.13	1285.64	–	2.55	Expt [21].
$Cs_3Cu_2Br_5$	9.920	11.191	13.918	1545.26	−3.129	2.092	[This work]
	9.730	11.100	13.785	1489.03	−1.384	–	Expt [45].
	9.578	10.967	13.628	1431.5	–	2.253	Expt [31].
	9.898	11.158	13.977	1543.65	–	2.10	Theo [32].
	9.65	10.99	13.73	1456.11	–	2.33	Expt [21].
$Cs_3Cu_2I_5$	10.504	11.888	14.779	1845.32	−2.855	2.292	[This work]
	10.325	11.785	14.541	1769.35	−1.106	–	Expt [45].
	10.467	11.876	14.703	1827.67	–	2.33	Theo [32].
	10.22	11.66	14.40	1715.99	–	2.44	Expt [21].

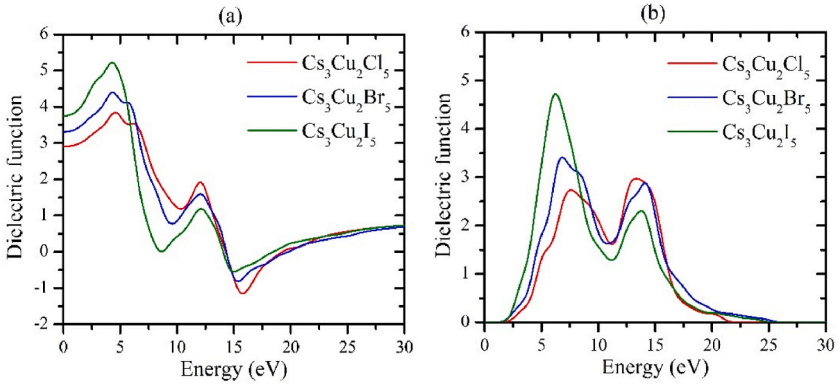

Fig. 2. The photon energy-dependent dielectric function of lead-free $Cs_3Cu_2X_5$ $(X = Cl, Br, I)$ perovskite, where (a) real parts and (b) imaginary parts.

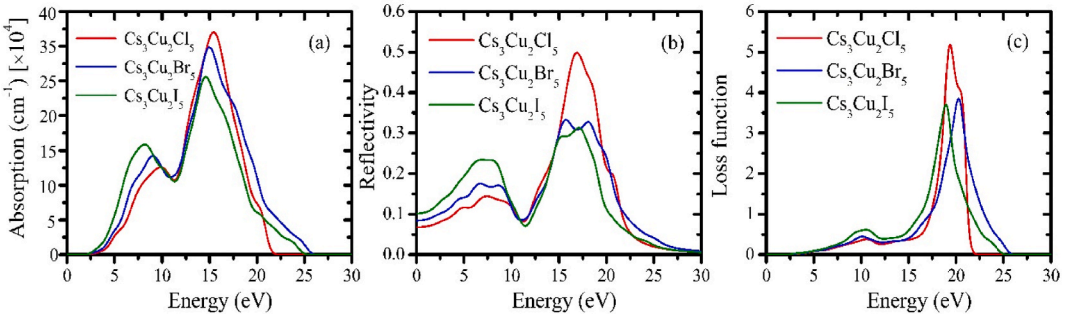

Fig. 3. The photon energy is dependent on (a) absorption, (b) reflectivity, and (c) loss function of lead-free $Cs_3Cu_2X_5$ $(X = Cl, Br, I)$ perovskite.

part and imaginary part of the studied materials optical conductivity characteristics are shown in Fig. 4(a) and (b), respectively. The change in optical conductivity is shown to be almost similar for all the materials. Additionally, the shapes of curves for optical conductivity and absorption spectra are similar. Conductivity spectra show that the inorganic compound $Cs_3Cu_2I_5$ has a more prominent peak than others, making it promising for a particular solar application [47]. In addition, we calculated the material's reflectivity, loss function, and refractive index; the findings are presented in Fig. 3b and c, and Fig. 5(a) and 5(b), correspondingly. Due to their low estimated reflectivity, reduced loss function, and strong refractivity, the compounds under consideration have the potential to be used in a variety of optoelectronic applications beyond their most well-known employment in solar systems. The high value of reflectivity in the UV area suggests that these compounds could be used as possible shielding materials to reduce solar heating by up to 18 eV.

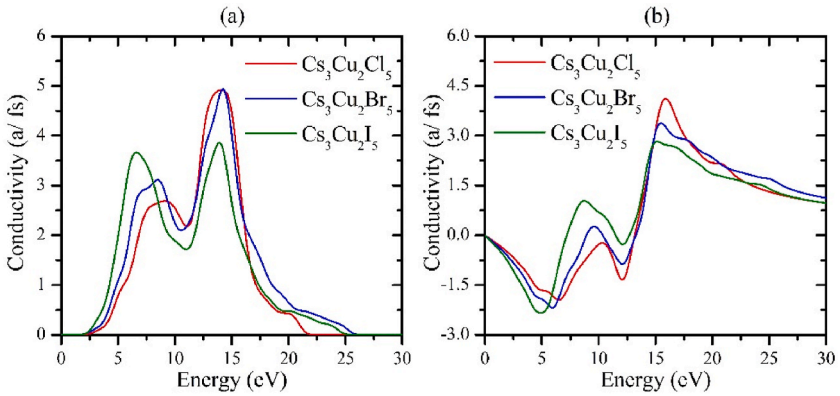

Fig. 4. The photon energy-dependent conductivity for lead-free $Cs_3Cu_2X_5$ $(X = Cl, Br, I)$ semiconductors, where (a) the real part and (b) the imaginary part.

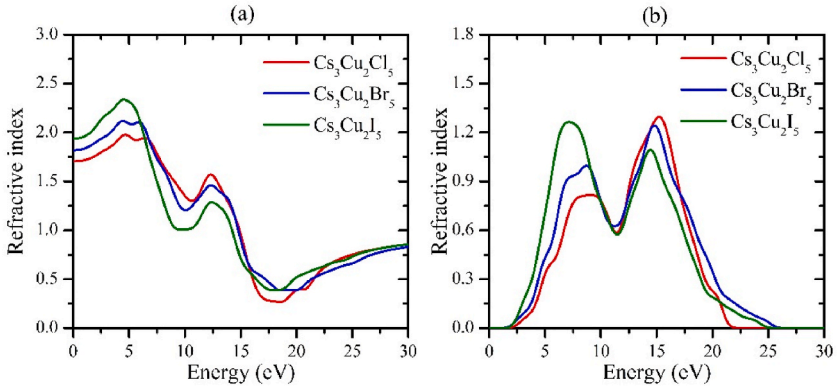

Fig. 5. The photon energy-dependent refractive index for lead-free $Cs_3Cu_2X_5$ $(X = Cl, Br, I)$ perovskites, where (a) the real part and (b) the imaginary part.

3.3. Electronic properties

The analysis of fundamental electrical and optical characteristics is crucial in understanding or forecasting the utilization of a material in a specific optoelectronic device, as its electronic properties have a strong connection to its optical properties [48]. In order to obtain the desired optoelectronic properties for particular applications, it is necessary to tune the electronic properties of comparable compounds. Herein, the band structure, DOS, and PDOS of the Cu-based inorganic compounds $Cs_3Cu_2X_5$ $(X = Cl, Br, I)$ have been investigated using the GGA-PBE method. Table 1 displays the simulated band gap results for the materials under consideration. The calculated electronic band gaps for halide perovskites are consistent with experimental data [21,30–32]. When Cl and I are used in place of Br, the band gap value increases. Additionally, among our studied compounds, $Cs_3Cu_2Br_5$ has the lowest band gap (2.092 eV), while $Cs_3Cu_2Cl_5$ has the highest band gap value (2.344 eV), indicating the materials' potential for photovoltaic applications.

Fig. 6(a) and (b) and (c) shows the simulated electronic band structures of $Cs_3Cu_2Cl_5$, $Cs_3Cu_2Br_5$, and $Cs_3Cu_2I_5$ perovskite, respectively. The horizontal dashed black line denotes the Fermi level, E_F. At the G point in the Brillion zone, both the valence band maximum (VBM) and conduction band minimum (CBM) are detected. This suggests that $Cs_3Cu_2X_5$ $(X = Cl, Br, I)$ materials are direct band gap semiconductors and $Cs_3Cu_2Br_5$ the lowest band gap value of 2.092 eV (Table 1). We also analyze the total density of states (TDOS) and partial densities of states (PDOS) to understand how atomic orbitals contribute to the formation of electronic states in the VBM and CBM. Fig. 7(a–c) shows the PDOS and TDOS of the studied perovskites. The results demonstrate that Cu in the 4s state (Cu-4s) and the s states of the halogens (I-5s, Br-4s, and Cl-3s) are the main contributors to the CBM, while Cu in the 3 d state (Cu-3d) and the p states of the halogens (I-5p, Br-4p, and Cl-3p) are the main contributors to the VBM [21,32]. Since halogen atoms simultaneously contribute to the VBM and CBM, it is simple to change the band gap of perovskites by substituting them with comparable atoms.

3.4. Mulliken atomic populations analysis

The analysis of Mulliken atomic population (MAP) is required for understanding the chemical bonding, bond overlap, and charge changes among the various atoms in a compound. The MAP is studied and listed in Table 2, which provides a deep understanding of the bonding characteristics of these perovskites [49]. Table 2 displays the positive charge of the Cs atom in the $Cs_3Cu_2Cl_5$ perovskite, while the negative charges of the Cu and Cl atoms indicate that the charge has been transferred from the Cs atom to the Cu and Cl atoms. Similarly charge transfer occurs from Cs to Cu and Br/I atoms in $Cs_3Cu_2Br_5$ and $Cs_3Cu_2I_5$ perovskites, respectively. The transferred charge for $Cs_3Cu_2Cl_5$, $Cs_3Cu_2Br_5$, and $Cs_3Cu_2I_5$ is respectively 0.2e and 0.5e, 0.37e and 0.18e, and 0.54e and 0.16e.

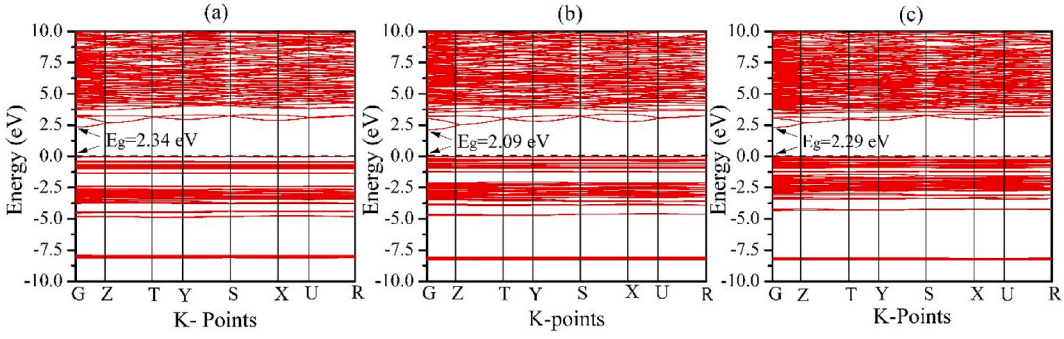

Fig. 6. Electronic band structures of $Cs_3Cu_2X_5$ perovskite, where (a) $Cs_3Cu_2Cl_5$, (b) $Cs_3Cu_2Br_5$, and (c) $Cs_3Cu_2I_5$.

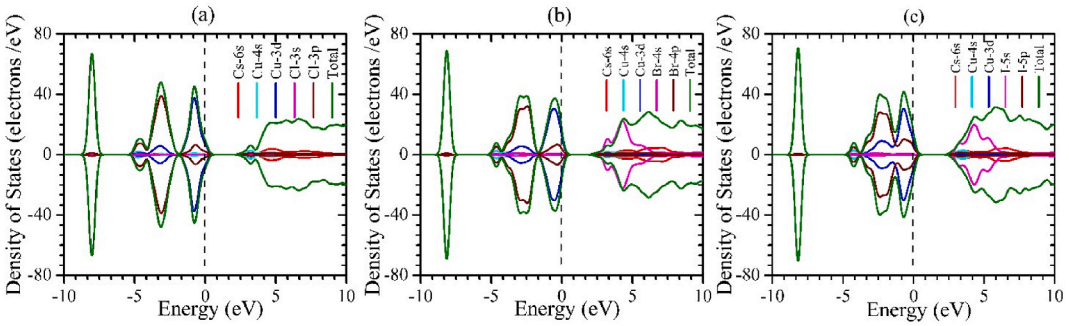

Fig. 7. Density of states (both partial and total) of $Cs_3Cu_2X_5$ perovskite, where (a) $Cs_3Cu_2Cl_5$, (b) $Cs_3Cu_2Br_5$, and (c) $Cs_3Cu_2I_5$.

Table 2
Mulliken atomic populations of $Cs_3Cu_2X_5$ $(X = Cl, Br, I)$ perovskite.

Compounds	Species	s	p	d	Total	Charge	Bond	Population	Lengths (Å)
$Cs_3Cu_2Cl_5$	Cs	1.03	2.99	0.00	4.02	0.96			
	Cu	0.36	0.35	4.93	5.60	−0.20	Cu–Cu	0.20	2.58
	Cl	0.97	2.78	0.00	3.75	−0.50	Cu–Cl	0.52	2.11
$Cs_3Cu_2Br_5$	Cs	1.08	3.14	0.00	4.23	0.55			
	Cu	0.32	0.42	4.95	5.69	−0.37	Cu–Cu	0.25	2.48
	Br	0.86	2.87	0.00	3.59	−0.18	Cu–Br	−0.12	2.48
$Cs_3Cu_2I_5$	Cs	1.08	3.11	0.00	4.19	0.62			
	Cu	0.36	0.47	4.95	5.77	−0.54	Cu–Cu	0.28	2.51
	I	0.87	2.70	0.00	3.58	−0.16	Cu–I	−0.02	2.65

This finding indicates that some ionic characteristics are present in all perovskites. Conversely, Table 2 illustrates the positive population of Cu–Cu and Cu–Cl bonds, indicating the covalent characteristics of these bonds within the compound $Cs_3Cu_2Cl_5$. Again, the population of Cu–Br and Cu–I bonds is negative, revealing the ionic nature of these bonds in $Cs_3Cu_2Br_5$ and $Cs_3Cu_2I_5$, respectively. Furthermore, the positive population of Cu–Cu bonds reveals the covalent nature of these bonds in the other two compounds.

3.5. Polycrystalline elastic constants

Acquiring knowledge of the elastic constants of engineering materials is a fundamental prerequisite for comprehending their diverse applications. The interatomic bonding and potential of a material are also determined by these factors [50]. It is possible to anticipate how an external force will impact a crystal by using elastic constants, which are closely related to the material's mechanical properties. These constants provide insight into a material's stability and stiffness. The CASTEP code employs the linear finite strain-stress function to determine the elastic constants of $Cs_3Cu_2X_5$ $(X = Cl, Br, I)$ [41]. Table 3 displays the nine different independent elastic constants (C_{ij}) for the orthorhombic $Cs_3Cu_2X_5$ $(X = Cl, Br, I)$ materials. There are three diagonals (C_{11}, C_{22}, C_{33}), three off-diagonals (C_{12}, C_{13}, C_{23}), and three shears (C_{44}, C_{55}, C_{66}) among the nine independent C_{ij}. The mechanical stability of a crystal structure is typically described using the Born-Huang criteria [51]. The orthorhombic structure must satisfy the well-known Born stability condition [52–54]:

$$C_{ij} > 0, [C_{11} + C_{22} + C_{33} + 2(C_{12} + C_{13} + C_{23})] > 0, [C_{11} + C_{22} - 2C_{12}] > 0, [C_{13} + C_{33} - 2C_{13}] > 0, [C_{22} + C_{33} - 2C_{23}] > 0 \quad (2)$$

All of the examined orthorhombic phases $Cs_3Cu_2X_5$ $(X = Cl, Br, I)$ are mechanically stable since the elastic constants we determined (Table 3) meet all of the stability criterions. In Fig. 8, a bar chart showing the variation in elastic constant of the examined perovskites, it is evident that $C_{22} > C_{11} > C_{33}$. Despite the lack of theoretical results of the elastic constant values of $Cs_3Cu_2X_5$ $(X = Cl, Br, I)$ phases in the literature, we expect our predictions to serve as a road map for further exploration of the $Cs_3Cu_2X_5$ $(X = Cl, Br, I)$ perovskite.

The degree to which a material can temporarily deform in response to an applied force is indicative of its elasticity. Elastic stiffness tensors can also be used to infer the bonding characteristics of solids.

The elastic constant C_{11} determines the stiffness of solids about the uniaxial strain e_1 in the [100] direction and also gives the

Table 3
Calculated elastic constants C_{ij} (GPa) for $Cs_3Cu_2X_5$ $(X = Cl, Br, I)$ perovskites.

Phase	C_{11}	C_{12}	C_{13}	C_{22}	C_{23}	C_{33}	C_{44}	C_{55}	C_{66}
$Cs_3Cu_2Cl_5$	11.840	5.067	2.682	18.831	8.168	7.179	2.589	3.131	0.607
$Cs_3Cu_2Br_5$	17.139	6.662	3.739	19.207	6.710	13.009	3.231	3.985	3.095
$Cs_3Cu_2I_5$	11.696	6.496	4.848	15.866	4.7902	11.810	2.482	2.752	2.941

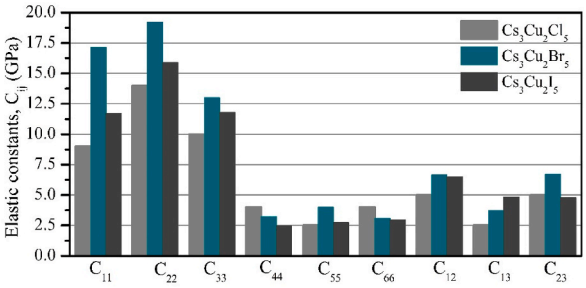

Fig. 8. The variation of the studied elastic constants for $Cs_3Cu_2X_5$ $(X = Cl, Br, I)$ perovskites.

elasticity in the length direction. Elastic constants C_{22} and C_{33} reflect the uniaxial strains e e_2 and e_3 in the [010] and [001] directions, respectively. From Tables 3 and it is clear that $C_{22} > C_{11} > C_{33}$, indicating stronger bonding along the [010] direction compared to the bonding along [100] and [001] directions. This result reveals that the compounds can be compressed along the c-axis of the crystal structure more easily than along the a- and b-axes. Moreover, $C_{22} > C_{11} > C_{33}$ reveals the anisotropic nature of the studied compounds.

3.6. Mechanical properties

The Voigt-Reuss-Hill formula uses zero-pressure elastic constants to calculate the shear modulus (G) and bulk modulus (B) [55,56]. The Voigt-Reuss-Hill (VRH) averaging approaches are usually used to determine the elastic moduli using the formulas (equations (3)–(8)) for $Cs_3Cu_2X_5$ $(X = Cl, Br, I)$ orthorhombic materials [57].

$$B_V = \frac{[C_{11} + C_{22} + C_{33} + 2(C_{12} + C_{13} + C_{23})]}{9} \tag{3}$$

$$G_V = \frac{[C_{11} + C_{22} + C_{33} + 3(C_{44} + C_{55} + C_{66}) - (C_{12} + C_{13} + C_{23})]}{15} \tag{4}$$

$$B = \frac{B_V + B_R}{2};\ G = \frac{G_V + G_R}{2} \tag{5}$$

$$E_{VRH} = \frac{9\ B_{VHR}G_{VHR}}{3B_{VHR} + G_{VHR}} \tag{6}$$

$$E = \frac{9BG}{3B + G} \tag{7}$$

$$\nu = \frac{3B_H - 2G_H}{2(3B_H + G_H)} \tag{8}$$

Here, the approximated bulk moduli for Voigt and Reuss are denoted by B_V and B_R, respectively. G_R and G_V represent the approximated bulk moduli for Reuss and Voigt, respectively.

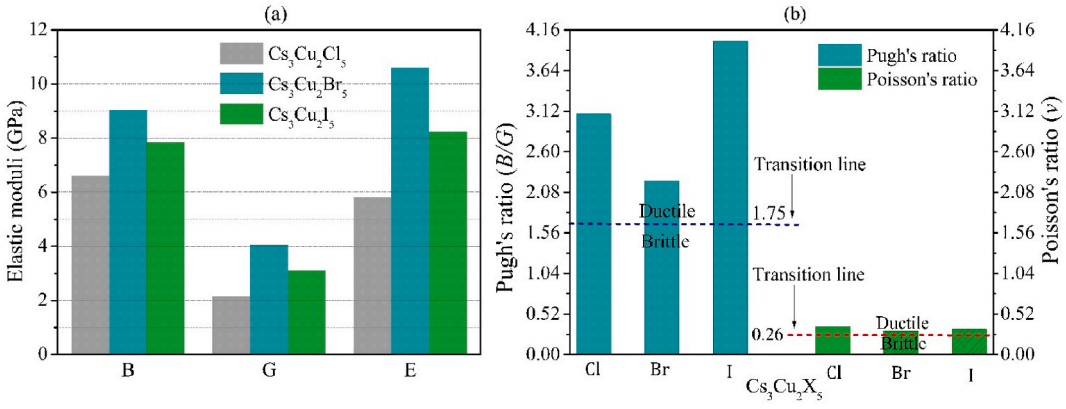

Fig. 9. Calculated (a) elastic moduli, (b) Pugh's ratio (B/G), and Poisson's ratio (ν), showing graphical representation of elastic moduli and ductile/brittle behavior of $Cs_3Cu_2X_5$ $(X = Cl, Br, I)$. The ductile-brittle transition line is represented by the horizontal dashed lines.

The calculated elastic moduli are shown in Fig. 9(a). Bulk modulus measures the average bonding strength between atoms in a solid [57]. Table 4 demonstrates that both phases have low bulk moduli ($B < 10$ GPa), indicating their soft nature and weak atom-to-atom bonds. The bonding strength of atoms provides the necessary resistance to volume deformation (bond length) when subjected to an external force. The shear modulus (G) indicates how well a material resists changing shape (bond angle) in response to external force. There is a strong correlation between the shear modulus (G) and the hardness of the materials. The material becomes more resistant to deformation as the shear modulus increases. The Young's modulus (E) determines a material's resistance to longitudinal stress. The stress-to-strain ratio can also be used to determine Young's modulus; a higher value of E implies that the material is stiffer.

In Fig. 10(a), a bar diagram shows the graphical representation of the calculated elastic moduli for all of the studied materials. It also shows that the shear modulus (G) is the limiting factor for mechanical stability across all phases, while the bulk modulus (B) is larger. The compound $Cs_3Cu_2Br_5$ displays superior shear resistance and a strong covalent bond in comparison to $Cs_3Cu_2Cl_5$ and $Cs_3Cu_2I_5$, as indicated by its higher shear modulus. The Pugh's ratio (B/G) is the ratio of the bulk modulus to the shear modulus and is used to determine implicitly whether a material is brittle or ductile [58]. The critical thermal shock coefficient (R) is inversely related to Young's modulus, hence this property affects a solid's resistance to thermal shock [59]. The resistance of thermal shock of a material increases with increasing R values. The selection of a thermal barrier coating (TBC) materials is based on its resistance to thermal stress. Notably, the investigated perovskites have relatively lower Young's moduli, making them potential TBC materials.

$\frac{B}{G} < 1.75 \rightarrow$A brittle material; $\frac{B}{G} > 1.75 \rightarrow$A ductile material.

Table 4 displays the computed values of B/G for each of the studied semiconductors, demonstrating that they are all ductile materials. Additionally, Poisson's ratio (υ), defined as the transverse to longitudinal ratio [60], has been used to differentiate brittle materials from ductile solids by Frantsevich et al. [33].

$\upsilon < 0.26 \rightarrow$A brittle material; $\upsilon > 0.26 \rightarrow$A ductile material.

Table 4 displays the calculated values of υ, which show that all of the investigated semiconductors are ductile. Cauchy pressure, defined as (C_{12}–C_{44}), can also be used to investigate the ductility and brittleness of solids [61]. Positive values of Cauchy pressure represent ductile materials, whereas negative values represent brittle materials. Our computed Cauchy pressure values reveal the ductile nature of all of the investigated materials. Therefore, the three indicators mentioned above indicate that the studied perovskites are ductile. The ductile/brittle behavior of the investigated perovskite materials is graphically depicted in Fig. 9(b). In addition, we conclude that the $Cs_3Cu_2X_5$ $(X = Cl, Br, I)$ perovskites are a good candidate for solar cells at low hydrostatic pressure and other optoelectronic devices at high hydrostatic pressure.

The value of Poisson's ratio (υ) can be used to infer the bonding properties of solids [62]. For ionic solids, υ is about 0.25, whereas for covalent materials, it is about 0.10 [63]. If the value of υ is between 0.25 and 0.5, we say that the substance has a center force solid. Since our estimated Poisson's ratio is within this range, highlighting the interatomic forces are most central. Cauchy pressure also predicted the nature of the atomic bonds in solids. Positive Cauchy pressure values are indicative of metallic bonds, whereas negative values indicate directional covalent bonds [64]. Using the estimated values of υ and Cauchy pressure, we can infer that perovskite materials exhibit both metallic and ionic bonding. Consequently, it is anticipated that the compounds under investigation will be metallic.

Hardness is a quantitative measure of a material's resistance to elastic deformation, plastic deformation, or failure due to external force. The values of E and υ can be used to hypothetically compute the hardness (H) of polycrystalline materials by utilizing the formula given in equation [65]:

$$H = \frac{(1-2\upsilon)E}{6(1+\upsilon)} \tag{9}$$

The estimated H values in Table 4 predict that all the phases are relatively soft materials, but $Cs_3Cu_2Br_5$ is less soft than $Cs_3Cu_2Cl_5$ and $Cs_3Cu_2I_5$ perovskites.

Elastic anisotropy influences a wide variety of physical phenomena, such as the formation of micro-scale cracks in ceramics, the emergence of plastic deformation in crystals, enhanced elastic instability, mechanical yield points, phase transitions, internal friction, charged defect mobility, etc. The anisotropic factor is used to describe the direction-dependent properties of the system. Anisotropy, denoted by the letter A, can be determined using the formula provided in Ref. [66].

$A = 1 \rightarrow$ isotropic material; $A \neq 1 \rightarrow$anisotropic material.

Table 4 displays the computed values of A for $Cs_3Cu_2X_5$ $(X = Cl, Br, I)$ compounds produced by the ELATE code [67]. According to Table 4, all of the investigated orthorhombic materials are anisotropic.

The elastic anisotropy can also be explained using contour diagrams in three dimensions. The direction dependence of E, G, and υ were visualised using the ELATE code [67] and are shown in Fig. 10(a–c). 3D contour plots were used to determine the type of anisotropy. Materials are considered isotropic if their 3D plots are perfectly spherical; otherwise, they are anisotropic. All of the materials under investigation have 3D figures that aren't perfectly spherical, which indicates a high degree of anisotropy. The

Table 4
The evaluated mechanical properties of $Cs_3Cu_2X_5$ $(X = Cl, Br, I)$.

Phase	B	G	E	ν	A	H	B/G	C_{12}–C_{44}
$Cs_3Cu_2Cl_5$	6.610	2.146	5.809	0.354	4.719	0.209	3.080	2.478
$Cs_3Cu_2Br_5$	9.040	4.069	10.614	0.304	1.625	0.532	2.221	3.431
$Cs_3Cu_2I_5$	7.853	3.113	8.248	0.325	1.652	0.363	4.014	2.366

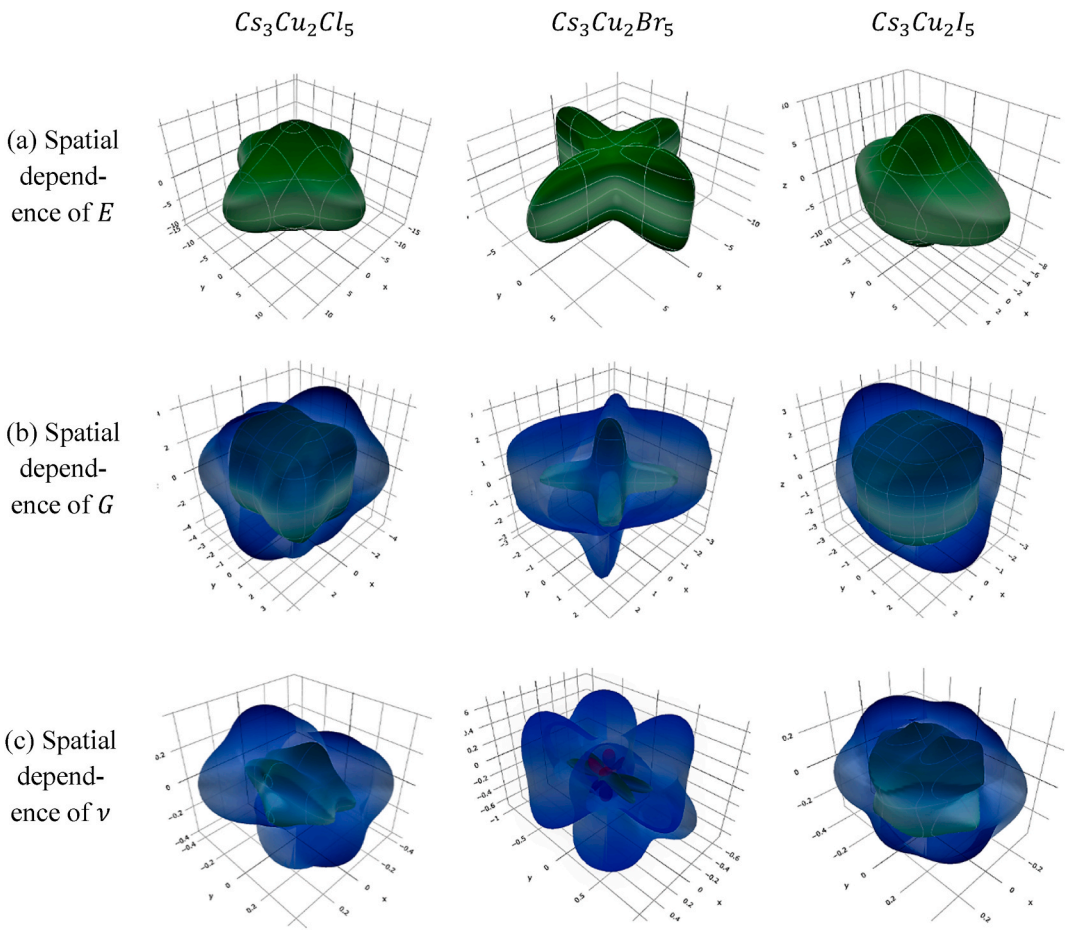

Fig. 10. 3D contour plots of (a) Young's modulus, (b) shear modulus, and (c) Poisson's ratio of $Cs_3Cu_2X_5$ $(X = Cl, Br, I)$ semiconductors.

outcomes of this investigation are in complete agreement with those of the anisotropy mentioned above.

3.7. Thermodynamics properties

Another crucial factor for solid materials is their thermodynamic features. These are crucial for comprehending how materials act under extreme conditions. Here we investigate the Debye temperature, Gr ü neisen parameter, melting temperature, and minimum thermal conductivity of $Cs_3Cu_2X_5$ $(X = Cl, Br, I)$ compounds. In Debye theory, the temperature at which a crystal achieves its strongest normal vibration mode is known as the Debye temperature (Θ_D). This temperature is reached when the unit cell length is equal to the phonon frequency wavelength. Vibrational response is measured by this quantity, and as a consequence it is related to phonons, specific heat, melting point, thermal conductivity, and thermal expansion [68]. In this investigation, we calculate the Debye temperature by utilizing the average sound velocity with the help of the following equation [69]:

$$\Theta_D = \frac{h}{K_B}\left[\frac{3n}{\pi}\left(\frac{N_A\rho}{M}\right)\right]^{\frac{1}{3}} \upsilon_m \tag{10}$$

Here, K_B stands for the Boltzmann constant, h for the Planck constant, N_A for the Avogadro number, for density, M for molecular weight, and n for the number of atoms in a unit cell.

The typical sound velocity in a crystal, denoted by υ_m, can be computed using the equation below:

$$\upsilon_m = \left[\frac{1}{3}\left(\frac{2}{\upsilon_t^3} + \frac{1}{\upsilon_l^3}\right)\right]^{\frac{-1}{3}} \tag{11}$$

Here, Navier's equation [70] is used to determine the longitudinal sound velocity (υ_l) and transverse sound velocity (υ_t) by using bulk modulus (B) and share modulus (G):

$$\upsilon_t = \left(\frac{G}{\rho}\right)^{\frac{1}{2}} \quad and \quad \upsilon_l = \left(\frac{3B + 4G}{3\rho}\right)^{\frac{1}{2}} \tag{12}$$

We also calculate the melting point of orthorhombic $Cs_3Cu_2X_5$ $(X = Cl, Br, I)$, we used the elastic constants C_{ij}, in the following formula [71]:

$$T_m = 354 + \frac{4.5(2C_{11} + C_{33})}{3} \tag{13}$$

In crystalline materials, the Gr ü neisen parameter (γ) illustrates the anharmonic effect, which describes the behavior of the phonon frequency and damping as a function of thermal expansion and temperature. Using Poisson's ratio, the Gr ü neisen parameter can be determined via the following equation [72]:

$$\gamma = \frac{3(1 + \upsilon)}{2(2 - 3\upsilon)} \tag{14}$$

We also estimated thermal conductivity, which is a crucial parameter for understanding the conduction of heat of a material. The thermal conductivity of a material is increased with a decrease in temperature to a specific limit is termed as the minimum thermal conductivity of that solid material. In this study, we also calculated the minimum thermal conductivity according to Clarke's equation [73]:

$$K_{min} = K_B \upsilon_m \left(\frac{M}{n\rho N_A}\right)^{-2/3} \tag{15}$$

Table 5 listed the computed values of ρ, ν_l, ν_t, ν_m, Θ_D, T_m, γ, and K_{min} for $Cs_3Cu_2Cl_5$, $Cs_3Cu_2Br_5$, and $Cs_3Cu_2I_5$ semiconductors. We are unable to compare our calculated values of Debye and melting temperature with other theoretical and experimental values because no such theoretical and experimental values are found in the literature. According to the calculated values listed in Table 5, $Cs_3Cu_2Br_5$ has a greater Debye temperature than the other studied compounds. Our predicted melting points for $Cs_3Cu_2Cl_5$, $Cs_3Cu_2Br_5$, and $Cs_3Cu_2I_5$ semiconductors are 400.289 K, 424.931 K, and 406.803 K, respectively. The estimated minimal thermal conductivity of all the studied perovskites are low at ambient conditions. However, $Cs_3Cu_2Br_5$ has a somewhat larger value than $Cs_3Cu_2Cl_5$ and $Cs_3Cu_2I_5$. Fig. 11(a) and (b) show the calculated Debye temperatures and melting temperatures for the compounds under study, respectively. As can be seen in Table 5, our estimates are in agreement with the rule of thumb, since substances investigated with low Debye temperatures also have low thermal conductivities. The phonon thermal conductivity is often lower when the Debye temperature falls, and vice versa. Consequently, the poor thermal conductivity indicated by the comparatively low values of Θ_D and K_{min} for $Cs_3Cu_2X_5$ $(X = Cl, Br, I)$, making them potentially useful as materials for thermal barrier coatings (TBC) [74].

4. Conclusions

In conclusion, the structural, optical, electronic, polycrystalline constants, mechanical, as well as thermodynamic features of three orthorhombic perovskites $Cs_3Cu_2X_5$ $(X = Cl, Br, I)$ have been investigated using the DFT-based first-principles method. The calculated lattice parameters are well consistent with the reported calculated and experimental results. The replacement of I by Br and Cl shifts the absorption peaks towards higher energies with a corresponding decrease in the strength of the first peaks. The studied semiconductors exhibit moderate photoconductivity, but the inorganic compound $Cs_3Cu_2I_5$ has a strong peak than others in the conductivity spectra, proving superior for a particular solar application. The investigated $Cs_3Cu_2X_5$ $(X = Cl, Br, I)$ perovskites are direct band gap semiconductors with the lowest band gap value of 2.092 eV for $Cs_3Cu_2Br_5$. The DOS reveals that Cu in its 4s state and halogens in their s states (I-5s, Br-4s, and Cl-3s) are the primary contributors to the CBM, while Cu in its 3 d state and halogens in their p states (I-5p, Br-4p, and Cl-3p) are the primary contributors to the VBM. The ionic and covalent properties of the $Cs_3Cu_2X_5$ $(X = Cl, Br, I)$ compounds have been confirmed by total charge density and Mulliken atomic population studies. All of the materials under consideration are mechanically stable and show anisotropic features. The ductility of all investigated perovskites is confirmed by three different indicators (Pugh's ratio, Poisson's ratio, and the Cauchy pressure). The predicted hardness values indicate that all phases will be soft, although $Cs_3Cu_2Br_5$ perovskites will be harder than $Cs_3Cu_2Cl_5$ and $Cs_3Cu_2I_5$. Our predicted melting points for the semiconductors $Cs_3Cu_2Cl_5$, $Cs_3Cu_2Br_5$, and $Cs_3Cu_2I_5$ are 400.289 K, 424.931 K, and 406.803 K, respectively. Consequently, the poor thermal conductivity indicated by the comparatively low values of Θ_D and K_{min} for $Cs_3Cu_2X_5$ $(X = Cl, Br, I)$, making them potentially useful as materials for thermal barrier coatings (TBC). The physiochemical characteristics of other 62-type orthorhombic perovskites should be thoroughly investigated, as this would be immensely beneficial for applications in optoelectronics and other related

Table 5
The computed density (ρ), transverse sound velocity $(\nu)_t$, longitudinal sound velocity (ν_l), average sound velocity (ν_m), melting temperature (T_m), and Debye temperature (Θ_D), Gr ü neisen parameter (γ), and minimum thermal conductivity (K_{min}) of $Cs_3Cu_2X_5$ $(X = Cl, Br, I)$ phases.

Phases	ρ (g/cm^3)	ν_l (m/s)	ν_t (m/s)	ν_m (m/s)	Θ_D (K)	T_m (K)	γ	K_{min} (W/mK)
$Cs_3Cu_2Cl_5$	3.270	1702.125	810.163	911.310	82.9	400.289	2.165	0.117
$Cs_3Cu_2Br_5$	3.937	1916.797	1016.613	1136.156	100	424.931	1.798	0.137
$Cs_3Cu_2I_5$	4.143	1702.142	866.819	971.334	80.7	406.803	1.939	0.104

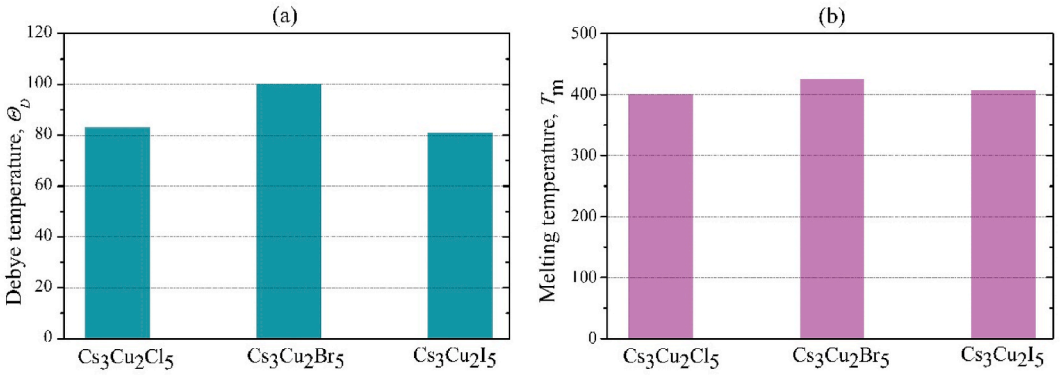

Fig. 11. The comparison of the calculated (a) Debye Temperature and (b) melting temperature of $Cs_3Cu_2X_5$ $(X = Cl, Br, I)$ semiconductors.

industries. Finally, we believe that our current investigation will serve as a strong motivation in future research and industrial development.

Author contribution statement

Md. Lokman Ali: Conceived and designed the experiments, Wrote the paper.
Mithun Khan: Performed the experiments, Analyzed and interpreted the data, Wrote the paper.
Md. Abdullah Al Asad, Md. Zahidur Rahaman: Analyzed and interpreted the data, contributed reagents, materials, analysis tools or data.

Data availability statement

Data will be made available on request.

Declaration of competing interest

The authors declare that they have no known competing financial interests or personal relationships that could have appeared to influence the work reported in this paper.

Acknowledgments

The authors are grateful to the Pabna University of Science and Technology, Bangladesh, for partial financial support during this research.

References

[1] M. Kumar, A. Raj, A. Kumar, A. Anshul, Recent advancement in inorganic-organic electron transport layers in perovskite solar cell: current status and future outlook, Opt. Mater. 111 (2021), 110565.
[2] W.S. Yangb, Iodide management in formamidinium-lead-halide-based perovskite layers for efficient solar cells, Science 356 (2017) 1376–1379.
[3] M.V. Kovalenko, L. Protesescu, M.I. Bodnarchuk, Properties and potential optoelectronic applications of lead halide perovskite nanocrystals, Science 358 (2017) 745–750.
[4] J. Chen, S. Zhou, S. Jin, H. Li, T. Zhai, Crystal organometal halide perovskite with promising optoelectronic applications, J. Mater. Chem. C 4 (2016) 11–27.
[5] M. Roknuzzaman, K. Ostrikov, H. Wang, A. Du, T. Tesfamichael, Electronic and optical properties of lead-free hybrid double perovskites for photovoltaic and optoelectronic applications, Sci. Rep. 7 (2017), 14025.
[6] M. Roknuzzaman, K. Ostrikov, K. Chandula Wasalathilake, C. Yan, H. Wang, T. Tesfamichael, Insight into lead-free organic-inorganic hybrid perovskites for photovoltaics and optoelectronics: a first-principles study, Org. Electron. 59 (2018) 99–106.
[7] M. Roknuzzaman, C. Zhang, K. Ostrikov, A. Du, H. Wang, L. Wang, T. Tesfamichael, Electronic and optical properties of lead-free hybrid double perovskites for photovoltaic and optoelectronic applications, Sci. Rep. 9 (2019) 718.
[8] O.M. Bakr, O.F. Mohammed, Intrinsic lead emissions in zero-dimensional Cs4PbBr6 nanocrystals, Science 355 (2017) 1260–1261.
[9] Y. Yang, J. You, Make perovskite solar cells stable, Nature 544 (2017) 155–156.
[10] W. Zhang, G.E. Eperon, H.J. Snaith, Shinning light on photoluminescence properties of metal halide perovskites, Nat. Energy 1 (2016), 16048.
[11] J.-P. Correa-Baena, M. Saliba, T. Buonassisi, M. Grätzel, A. Abate, W. Tress, A. Hagfeldt, Promises and challenges of perovskite solar cells, Science 358 (2017) 739–744.
[12] M. Lira-Cantú, Nanostructured materials for photovoltaic energy, Nat. Energy 2 (2017), 17115.
[13] C. LungChien, T. Zong-Liang, C. Wei-Wen, J. Warm white light-emiting diodes using organic-inorganic halide perovskite materials coated YAG:Ce3+ phosphors, Ceram. Int. 44 (2018) 3868–3872.
[14] J.J. Luo, M.C. Hu, G.D. Niu, J. Tang, Lead-free halide perovskites variants as phosphors toward light-emitting applications, ACS Appl. Mater. Interfaces 11 (2019) 31575–31584.
[15] Y. Li, Z. Shi, L. Lei, S. Li, D. Yang, D. Wu, T. Xu, Y. Tian, Y. Lu, Y. Wang, L. Zhang, X. Li, Y. Zhang, G. Du, C. Shan, Ultrastable lead-free double perovskite photodetectors with imaging capability, Adv. Mater. Interfac. 6 (2019), 1900188.

[16] N.M. Nobin, M. Khan, M.L. Ali, An atomistic modeling study of high-throughput RVO3 (R = La, Nd) perovskites for efficient solar energy conversion materials, Phys. B Condens. Matter 660 (2023), 414879.
[17] M.G. Brik, Comparative first-principles calculations of electronic, optical, and elastic anisotropy properties of CsXBr3 (X= Ca, Ge, Sn) crystals, Solid State Commun. 151 (2011) 1733.
[18] B. Yang, J.S. Chen, F. Hong, X. Mao, K.B. Zheng, S.Q. Yang, Y.J. Li, T. Pullerits, W.Q. Deng, K.L. Han, Angew, lead-free, air-stable all-inorganic cesium bismuth halide perovskite nanocrystals, Chem., Int. Ed 56 (2017) 12471–12475.
[19] T. Jun, K. Sim, S. Iimura, M. Sasase, H. Kamioka, J. Kim, H. Hosono, Lead-free highly efficient blue-emitting Cs3Cu2I5 with 0D electronic structure, Adv. Mater. 30 (2018), 1804547.
[20] J. Lv, X. Lu, X. Li, M. Xu, J. Zhong, X. Zheng, Q. Zhang, Epitaxial grouth of lead-free 2D Cs3Cu2I5 perovskite for high-performance UV photodetectors, Small 18 (27) (2022), 2201715.
[21] Z. Luo, Q. Li, L. Zhang, X. Wu, L. Tan, C. Zou, Z. Quan, 0D Cs3Cu2X5 (X= I, Br, and Cl) nanocrystals: colloidal syntheses and optical properties, Small 16 (3) (2020), 1905226.
[22] F. Zeng, Y. Guo, W. Hu, Y. Tan, X. Zhang, J. Feng, X. Tang, Opportunity of the lead-free all-inorganic Cs3Cu2I5 perovskite film for memristor and neuromorphic computing applications, ACS Appl. Mater. Interfaces 12 (2020) 23094–23101.
[23] D. Yuan, ACS Appl. Mater. Interfaces 12 (2020) 38333–38340.
[24] Y. Pan, Y. Lin, G. Liu, J. Zhang, Influence of transition metal on the mechanical and thermodynamic properties of IrAl thermal barrier coating, Vacuum 174 (2020), 109203.
[25] M.L. Ali, M.M. Billah, M. Khan, M.N.M. Nobin, M.Z. Rahaman, Pressure-induced physical properties of alkali metal chlorides Rb2NbCl6, Density Func. Theory Stud. 13 (2023), 065110.
[26] C.K. Zhou, Y. Tian, M.C. Wang, A. Rose, T. Besara, N.K. Doyle, Z. Yuan, J.C. Wang, R. Clark, Y.Y. Hu, T. Siegrist, S.C. Lin, B.W. Ma, Angew. Chem. Int. Ed. 56 (2017) 9018.
[27] C.K. Zhou, H.R. Lin, Y. Tian, Z. Yuan, R. Clark, B.H. Chen, L.J. van de Burgt, J.C. Wang, Y. Zhou, K. Hanson, Q.J. Meisner, J. Neu, T. Besara, T. Siegrist, E. Lambers, P. Djurovich, B.W. Ma, Chem. Sci. 9 (2018) 586.
[28] M.A. Haque, A.N. Gandi, R. Mohanraman, Y.K. Weng, B. Davaasuren, A.H. Emwas, C. Combe, D. Baran, A. Rothenberger, U. Schwingenschlogl, H.N. Alshareef, S. Dong, T. Wu, Adv. Funct. Mater. 29 (2019), 1809166.
[29] X.T. Zhang, C.C. Wang, Y. Zhang, X.Y. Zhang, S.X. Wang, M. Lu, H.N. Cui, S.V. Kershaw, W.W. Yu, A.L. Rogach, ACS Energy Lett. 4 (2019) 242.
[30] L. Xie, B. Chen, F. Zhang, Z. Zhao, X. Wang, L. Shi, Y. Liu, L. Huang, R. Liu, B. Zou, Y. Wang, Highly luminescent and stable lead-free cesium copper halide perovskite powders for UV-pumped phosphor-converted light-emitting diodes, Photon. Res. 8 (2020) 768–775.
[31] X. Zheng, J. Huang, Y. Liu, T. Wang, Z. Wang, B. Teng, S. Ji, Stable lead-free blue-emitting Cs3Cu2Br5 single crystal with self-trap exciton emission for optoelectronics, Adv. Photonic. Res. 3 (2022), 2100289.
[32] Z. Lan, J. Meng, K. Zheng, I. Castelli, Exploring the intrinsic point defects in cesium copper halides, J. Phys. Chem. C 125 (2) (2021) 1592–1598.
[33] J.C. Stewart, D.M. Segall, J.C. Pickard, P.J. Hasnip, M.I. Probert, K. Refson, M.C. Payne, First principles methods using CASTEP, Cryst. Mater. 220 (2005) 567–570.
[34] U.K. Chowdhury, M.A. Rahman, M.A. Rahman, M.T.H. Bhuiyan, M.L. Ali, Ab initio study on structural, elastic, electronic and optical properties of cuprate based superconductor, Cogent. Phys. 3 (2016), 1231361.
[35] W. Kohn, L.J. Sham, Self-consistent equations including exchange and correlation effects, Phys. Rev. 140 (1965) A1133.
[36] P.P. John, A. Ruzsinszky, I. Gabor, Csonka, A. Oleg, E. Gustavo Vydrov, A.S. Lucian, A. Constantin, X. Zhou, K. Burke, Phys. Rev. Lett. 101 (2008), 239702.
[37] P.P. John, K. Burke, M. Ernzerhof, Generalized gradient approximation made simple, Phys. Rev. Lett. 77 (1996) 3865.
[38] C.J. Pickard, M.C. Payne, Second-order k.p perturbation theory with Vanderbilt pseudopotentials and plane waves, Phys. Rev. B 62 (2000) 4383–4388.
[39] B. Max, Mathematical proceedings of the cambridge philosophical society, Int. Math. Proc. Cambridge Philos. Soc. 36 (1940) 160–172.
[40] H.F. Thomas, J. Almlof, General methods for geometry and wave function optimization, J. Phys. Chem. 96 (1992) 9768–9774.
[41] C.Z. Fan, S.Y. Zeng, L.X. Li, Z.J. Zhan, R.P. Liu, W.K. Wang, P. Zhang, Y.G. Yao, Potential superhard osmium dinitride with fluride and pyrite structure: first-principles calculations, Phys. Rev. B 74 (2006), 125118.
[42] V. Woldemar, A Critical Study of the Elastic Properties and Stability of Heusler Compounds: Phase Change and Tetragonal X2YZ Compounds, Lehrbuch der Kristallphysik (Teubner, Leipzig, 1928, p. 962.
[43] Z. Hashin, S. Shtrikman, A variational approach to the theory of the elastic behavior of polycrystals, J. Mech. Phys. Solid. 10 (1962) 343–352.
[44] H. Richard, The elastic behavior of a crystalline aggregate, Proc. Phys. Soc. 65 (1952) 349–354.
[45] S. Hull, P. Berastegui, Crystal structure and ionic conductivities of the silver and copper monohakides, J. Solid State Chem. 177 (2004) 3156–3173.
[46] Y. Pan, E. Yu, Structure and stabilities of carbon chain clusters influenced by atomic antimony, Int. J. Energy Res. 46 (14) (2022) 19678–19685.
[47] L. Lian, M. Zheng, P. Zhang, Z. Zheng, K. Du, W. Lei, J. Zhang, Photophysics in Cs3Cu2X5 (X = Cl, Br, or I): highly luminescent self-trapped excitons from local structure summarization, Chem. Mater. 32 (8) (2020) 3462–3468.
[48] M.D. Segall, R. Shah, C.J. Pickard, M.C. Payne, Population analysis of plane-wave electronic structure calculations of bulk materials, Phys. Rev. B 54 (1996), 16317.
[49] C.A. Ponce, R.A. Casali, M.A. Caravaca, Ab initio study of mechanical and thermacoustic properties of tough ceramics, J. Phys. Condens. Matter 20 (2008), 045213.
[50] M.N. Islam, J. Podder, M.L. Ali, The effect of metal substitution in CsSnI3 perovskites with enhanced optoelectronic and photovoltaic properties, RSC Adv. 11 (2021) 39553–39563.
[51] G. SinKo, N. Smirnov, Ab initio calculations of elastic constants and thermodynamic properties of bcc, fcc, and hcp Al crystals under pressure, J. Phys. Condens. Matter 14 (2002) 6989–7005.
[52] G. SinKo, N. Smirnov, Anomalous self-energy and Fermi surface quasisplitting in the vicinity of a ferromagnetic instability, Phys. Rev. B 71 (2005), 214108.
[53] Z.J. Wu, E.J. Zhao, H.P. Xiang, X.F. Hao, X.J. Liu, Crystal structure and elastic properties of superhard IrN2 and IrN3 from first principles, J. Meng, Phys. Rev. B 76 (2007), 054115.
[54] X. Wang, H. Xiang, X. Sum, J. Liu, F. Hou, Y. Zhou, Mechanical properties and damage tolerance of bulk Yb3Al5O12 ceramic, J. Mater. Sci. Technol. 31 (2015) 369–374.
[55] W. Voigt, A Critical Study of the Elastic Properties and Stability of Heusler Compounds: Phase Change and Tetragonal X2YZ Compounds, Lehrbuch Der Kristallphysik (Mit Ausschluss Der Kristalloptik). Nachdruck der ersten Aufl, ed., B.G. Teubner J.W. Edwards, Leipzig Berlin, 1928.
[56] A. Bouhemadou, First-principles study of structural, electronic and elastic properties of Nb4AlC3, Rev. Brasileira Fisioterapia 40 (2010) 52–57.
[57] I.N. Frantsevich, F.F. Voronov, S.A. Bokuta, Elastic constants and elastic moduli of metals and insulators handbook, in: Frantsevich IN, Naukova Dumka, Kiev, 1983, pp. 60–180.
[58] A.A. Maradudin, E.W. Montroll, G.H. Weis, I.P. Ipatova, Theory of Lattice Dynamics in the Harmonic Approximation, Academic Press, New York, 1971.
[59] S.F. Pugh, XCII. Relations between the elastic moduli and the plastic properties of polycrystalline pure metals, Phil. Mag. 45 (1954) 823–843.
[60] D.G. Pettifor, Theoretical predictions of structure and related properties of intermetallics, Mater. Sci. Technol. 8 (1992) 345–349.
[61] Y. Cao, J. Zhu, Y. Liu, Z. Nong, Z. Lai, First-principles studies of the structural, elastic, electronic and thermal properties of Ni3Si, Comput. Mater. Sci. 69 (2013) 40–45.
[62] K.M. Hossain, M.Z. Hasan, M.L. Ali, Narrowing bandgap and enhanced mechanical and optoelectronic properties of perovskite halides: effects of metal doping, AIP Adv. 11 (2021), 015052.
[63] Y. Liu, W. Hu, D. Li, X. Zeng, C. Xu, X. Yang, First-principles investigation of structural and electronic properties of MgCu2 Laves phase under pressure, Intermetallics 31 (2012) 257–263.
[64] X.Q. Chen, H. Niu, D. Li, Y. Li, Modeling hardness of polycrystalline materials and bulk metallic glasses, Intermetallics 19 (2011) 1275–1281.

[65] K.M. Hossain, M.Z. Hasan, M.L. Ali, Understanding the influences of Mg doping on the physical properties of SrMoO3 perovskite, Results Phys. 19 (2020), 103337.
[66] M.L. Ali, M.Z. Rahman, Investigation of different physical aspects such as structural, mechanical, optical properties and Debye temperature of Fe2ScM (M = P and As) semiconductors: a DFT-based first principles study I, J. Mod. Phys. B 32 (2018), 1850121.
[67] R. Gaillac, P. Pullumbi, F.X. Coudert, ELATE: an open-source online application for analysis and visualization of elastic tensors, J. Phys. Condens. Matter 28 (2016), 275201.
[68] S. Aydin, M. Simsek, First-principles calculations of MnB2, TcB2, and ReB2, Phys. Rev. B 80 (13) (2009), 134107.
[69] O.L. Anderson, A simplified method for calculating the Debye temperature from elastic constants, J. Phys. Chem. Solid. 24 (1963) 909–917.
[70] M.E. Fine, L.D. Brown, H.L. Marcus, The properties of elasticity, thermology, and anisotropy in pd-based alloys, Scripta Metall. Mater. 18 (1984) 951–956.
[71] V. Belomestnykh, E. Tesleva, Interrelation between anharmonicity and lateral strain in quasi-isotropic polycrystalline solids, Tech. Phys. 49 (2004) 98–100.
[72] D.R. Clarke, Materials selection guideline for low thermal conductivity thermal barrier coatings technology, Surf. Coat. Technol. 63 (2003) 67–74.
[73] M.L. Ali, M.Z. Rahaman, The structural, elastic and optical properties of ScM (, Cu, Ag, Hg) intermetallic compounds under pressure by ab initio simulations, Int. J. Mater. Sci. Appl. 5 (2016) 202–206.
[74] M.Z. Rahaman, M.L. Ali, Insight into the physical properties of two niobium-based compounds, Nb3Be and Nb3Be2, via a first principles calculation, Chin. J. Phys. 56 (2018) 1386–1393.